SIMPLE ONE-DIMENSIONAL CALCULATION OF HALL THRUSTER FLOWFIELDS

Hirokazu Tahara, Takashi Fujioka, Atsushi Shirasakiand Takao Yoshikawa
Graduate School of Engineering Science, Osaka University
1-3, Machikaneyama, Toyonaka, Osaka 560-8531, JAPAN
Phone: +81-6-6850-6178
Fax: +81-6-6850-6179
E-mail: tahara@me.es.osaka-u.ac.jp

Abstract

Low-power Hall thruster flowfields were calculated using a simple one-dimensional model to understand plasma characteristics and ion acceleration processes and to predict thruster performance. The influences of magnetic field strength and acceleration channel length were mainly examined. The model includes first ionization by direct electron-neutral collisions, electron-neutral elastic collisions, Bohm diffusion (anomalous diffusion); channel wall losses of ion flux and electron energy flux with secondary electron emission effect. The thruster model for calculation is the THT-IV low power thruster developed in Osaka University. Generally, ions were produced in an upstream region from the anode to some axial location of the acceleration channel, and then they were intensively accelerated in a region downstream just from the ionization region. When the magnetic field strength increased in the channel, ionization occurred in a more upstream region, and ion acceleration began in the same region; that is, ionization and acceleration overlapped in the relatively long region. On the other hand, with a weak magnetic field ion production and acceleration, intensively and efficiently, occurred in their thin regions. With too short channel, ionization began downstream just from the anode, and then ion acceleration also occurred in the same region. In large channel length, the channel was long enough to produce a fully-ionized plasma, and efficient ion production and acceleration occurred. The calculated thruster performance agreed with the calculated voltage utilization efficiency, plasma plume divergent half-angle and energy balance characteristics as well as the distributions of physical properties in the channel. However, because the measured performance characteristics did not agree well with the calculated ones, we need to improve the present calculation model. Furthermore, we tried to include unclear anomalous electron diffusions by changing a Bohm diffusion coefficient at each high magnetic field strength in order to fit a calculated performance to the measured one. The calculated discharge current almost equaled the measured one, and the thrust characteristic also agreed well with the measured one.

1. Introduction

The closed-electron-drift Hall-effect thruster is a promising propulsion device in space. The performance has been improved in Russia since 1960s[1]. Because 1-2 kW class Hall thrusters can achieve a high performance of thrust 50-100 mN and thrust efficiency 40-50 % at specific impulses of 1000-2000 sec, they are expected to be used as main thrusters for near-earth missions in the United States and Europe[2],[3]. Even in Japan, the high performance attracts attention of mission planners[4]-[8]. However, the detailed physics on plasma characteristics and ion acceleration processes is still unclear. We need both basic and practical studies in order to improve Hall thruster performance by understanding inner physical phenomena.

In Osaka University, an experimental facility was constructed in 1997 to study plasma production and acceleration processes and unstable operational phenomena in low power Hall thrusters and also to examine spacecraft and plasma plume interactions[4],[5]. Basic experiments were made using THT-series low-power Hall thrusters to obtain fundamental operational characteristics. The influences of material, width and length of acceleration channel on thruster performance were mainly investigated[6],[7]. As a result, the THT-IIIA thruster could be stably operated in a wide range of magnetic field strength. A high thrust efficiency was achieved with a low discharge current and a high thrust for a preferable magnetic field strength regardless of discharge voltage at a constant mass flow rate. Furthermore, one-dimensional thruster flowfield calculation was carried out[7],[8]. The calculated thruster performance roughly agreed with experimental one. Currently, a joint development of low power Hall thrusters between Osaka University and Ishikawajima-

Harima Heavy Industries Co., Ltd. started in 1999[9]-[11]. With a new thruster with many considerations, long stable operations were achieved. In all

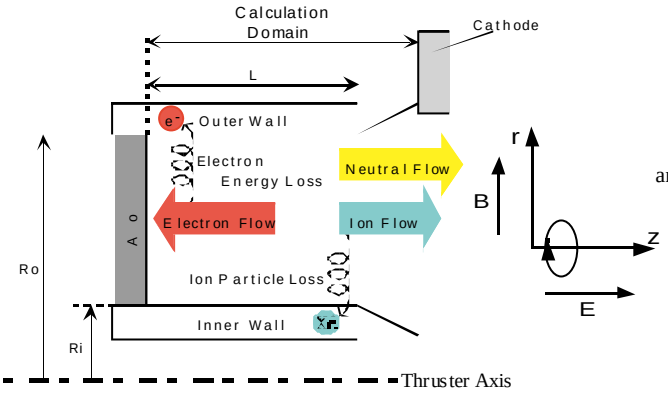

Fig.1 Calculation model of one-dimensional Hall thruster flowfield.

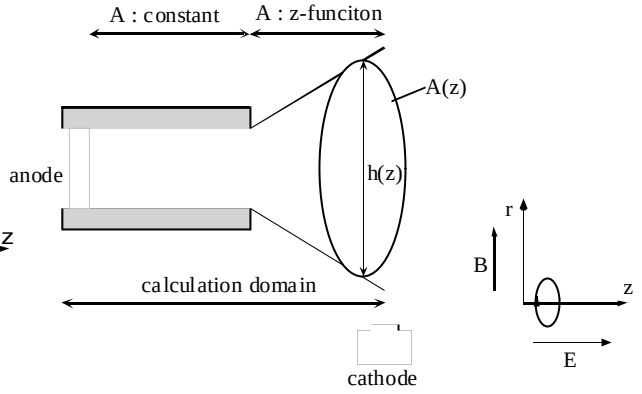

Fig.2 Calculation model of quasi-one-dimensional exhaust plasma plume.

experiments at 200-400 V with 1.5-3 mg/s, the thrust and the specific impulse ranged from 15 to 70 mN and from 1100 to 2300 sec, respectively, in a low electric power range of 300-1300 W. The thrust efficiency reached 55 %. Hence, a large map of the thruster performance was successfully made. The thermal characteristics were also examined with data of both measured and calculated temperatures in the thruster body. As a result, thermally safe conditions were achieved with all input powers.

In the present study, low-power Hall thruster flowfields are calculated using a simple one-dimensional model to understand plasma characteristics and ion acceleration processes and to predict thruster performance. The influences of magnetic field strength and acceleration channel length are mainly examined. The model includes first ionization by direct electron-neutral collisions, electron-neutral elastic collisions, Bohm diffusion (anomalous diffusion); channel wall losses of ion flux and electron energy flux with secondary electron emission effect. The thruster model for calculation is the THT-IV low power thruster developed in Osaka University[11]. Several physical properties in the acceleration channel are calculated, and voltage utilization efficiency, plasma plume divergent half-angle and energy balance characteristics are evaluated. The calculated thruster performance is compared with the measured one. Furthermore, we try to include unclear anomalous electron diffusions by changing a Bohm diffusion coefficient at each high magnetic field strength in order to fit a calculated performance to the measured one.

2. One-Dimensional Flowfield Calculation

Hall thruster flowfields are calculated using a simple one-dimensional model as shown in Fig.1. The model includes first ionization by direct electron-neutral collisions, electron-neutral elastic collisions, Bohm diffusion (anomalous diffusion); channel wall losses of ion flux and electron energy flux with secondary electron emission effect, but without electron conduction enhanced near the channel wall[7],[8],[12].

The following conservation equations of mass, axial momentum of ions, and energy of electrons are made.

Mass:

$$\frac{d(n_e V_i)}{dz} = -n_e V_i \frac{1}{A}\frac{dA}{dz} + n_e \nu_{ion} - n_e \nu_{wall} \qquad (1)$$

where n_e is electron (ion) number density, V_i axial ion velocity, a cross-sectional area of acceleration channel, $_{ion}$ ionization collision frequency, and $_{wall}$ frequency of ion flux loss to channel wall.

Ion momentum in axial direction:

$$\frac{d(n_e V_i^2)}{dz} = -n_e V_i^2 \frac{1}{A}\frac{dA}{dz} + \frac{e}{m_i} n_e E + n_e \nu_{ion} V_n - n_e \nu_{wall} V_i \qquad (2)$$

where e is electron charge, m_i ion mass, E electric field, and V_n axial neutral velocity.

Electron energy:

$$\frac{\partial e_t}{\partial t}+\frac{\partial}{\partial z}[V_e\cdot(e_t+p_e)]=-V_e\cdot(e_t+p_e)\frac{1}{A}\frac{dA}{dx}-en_eV_eE-\alpha_i n_e\nu_{ion}E_i$$
$$-n_e\nu_{en}\frac{2m_e}{m_n}\frac{3}{2}k(T_e-T_n)-n_e\nu_{wallE}E' \qquad (3)$$
$$e_t=n_e(\frac{3}{2}kT_e+\frac{1}{2}m_ev_e^2)\cong\frac{3}{2}n_ekT_e\ ;\ p_e=n_ekT_e$$

where e_t is internal energy of electron, p_e electron pressure, k Boltzmann factor, V_e axial electron velocity, m_e electron mass, m_n neutral mass, T_e electron temperature, T_n neutral temperature, E_i ionization energy, $_i$ factor of additional energy loss by ionization (for example, excitation losses), $_{wallE}$ frequency of electron energy loss to channel wall, and E' electron energy loss to channel wall.

Additional equations of axial motion of electrons, current continuity, and global mass continuity etc. are introduced.

Axial motion of electrons:

$$V_e=-\mu_eE\ ;\ \mu_e=\frac{e}{m_e}\frac{\nu_{en}}{\omega_B^2+\nu_{en}^2}+\alpha_B\frac{1}{B}\cong\frac{e}{m_e}\frac{\nu_{en}}{\omega_B^2}+\alpha_B\frac{1}{B};\ \omega_B=\frac{eB}{m_e} \qquad (4)$$

where $_e$ is axial mobility of electrons, $_B$ electron cyclotron frequency, $_{en}$ electron-neutral elastic collision frequency, $_B$ Bohm diffusion coefficient, and B magnetic field strength.

Current continuity:

$$J_d=en_e(V_i-V_e)A \qquad (5)$$

where J_d is discharge current.

The electric field is calculated from Eqs.(4) and (5) as follows.

$$E=\frac{1}{\mu_e}(\frac{J_d}{en_eA}-V_i) \qquad (6)$$

The discharge voltage is evaluated from integration of electric field as follows:

$$V_d=\int_0^{L'}Edz \qquad (7)$$

where V_d is discharge voltage, and L' distance from cathode to anode.

The azimuthal electron current (Hall current) is also calculated as follows:

$$J_{e\theta}=\frac{\omega_B}{\nu_{en}+\alpha_B\omega_B}J_{ez}=\Omega J_{ez} \qquad (8)$$

where J_e and J_{ez} are azimuthal and axial electron currents, respectively, and electron Hall parameter.

Also, the following equation of global mass continuity is implicitly used to obtain neutral number density:

$$\dot{m}=A(m_nn_nV_n-m_in_iV_i) \qquad (9)$$

where $\dot{m}$ is mass flow rate, and n_n neutral number density.

As shown in Fig.2, the exhaust plasma plume outside the acceleration channel is modeled as divergent nozzle expansion without wall losses. The divergent angle is determined from a ratio of magnetosonic velocity to axial ion velocity at the channel exit as follows:

$$\frac{1}{A}\frac{dA}{dz}=\frac{1}{h}\frac{dh}{dz};\ \frac{1}{A}\frac{dA}{dz}=\frac{2}{h}\tan\theta;\ \tan\theta=\frac{\sqrt{\frac{5T_{e\ channel-exit}}{3m_i}}}{V_{ichannel-exit}} \qquad (10)$$

where h is average length related to cross-sectional area of divergent nozzle, divergent half-angle, $T_{e\ channel-exit}$ and $V_{i\ channel-exit}$ electron temperature and axial ion velocity, respectively, at the channel exit.

We also assume that velocity of neutrals are constant (thermal velocity) and that temperatures of neutrals, ions, the channel wall and secondary electrons emitted from the wall are constant (1000 K).

$$V_n=constant(=\left(\frac{5}{3}\frac{kT_n}{M_n}\right)^{1/2}) \qquad (11)$$

$$T_n=T_i=T_{wall}=T_{se}=constant(=1000K) \qquad (12)$$

where T_{wall} is channel wall temperature, and T_{se} secondary-emission-electron temperature.

At the upstream end (at the anode), the velocity of ions is assumed to be a sonic velocity, and an ionization degree of 0.005 is given. The electron temperature is extrapolated upstream. At the downstream end (at the cathode), the electron number density and the axial ion velocity are extrapolated downstream.

The electron temperature is fixed to 3 eV, corresponding to the temperature of electrons emitted from a hollow cathode.

The frequency of ion flux loss to channel wall $_{wall}$ is determined as follows:

$$\nu_{wall} = \alpha_w \times \frac{1}{W} \times 2 \times \frac{1}{n_e} \times \Gamma_i \tag{13}$$

$$\Gamma_i = \begin{cases} \left(\frac{kT_e}{2\pi m_e}\right)^{\frac{1}{2}} n_e \exp\left(\frac{e\phi_w}{kT_e}\right)(1-\delta) & (\phi_w < 0) \\ \left(\frac{kT_e}{2\pi m_e}\right)^{\frac{1}{2}} n_e & (\phi_w \geq 0) \end{cases} \tag{14}$$

where $_w$ is attenuation factor, W acceleration channel width, $_i$ ion (electron) flux to channel wall, $_w$ wall potential on plasma potential, and secondary electron emission coefficient.

The frequency of electron energy loss to channel wall $_{wallE}$ is determined as follows:

$$\nu_{wallE} \times E' = \alpha_w \times \frac{1}{W} \times 2 \times \frac{1}{n_e} \times \Gamma_e \times E' \tag{15}$$

$$\Gamma_e \times E' = \begin{cases} \left(\frac{kT_e}{2\pi m_e}\right)^{\frac{1}{2}} n_e \exp\left(\frac{e\phi_w}{kT_e}\right)\left[(2kT_e - e\phi_w) - \delta(2kT_{sec} - e\phi_w)\right] & (\phi_w < 0) \\ \left(\frac{kT_e}{2\pi m_e}\right)^{\frac{1}{2}} n_e 2k(T_e - T_{sec}) & (\phi_w \geq 0) \end{cases} \tag{16}$$

where $_e$ is electron flux to channel wall.

Both the wall losses depend on sheath structure in front of acceleration channel wall. The wall potential is determined with the sheath theory with negative potential as follows.

$$\phi_w = -\frac{kT_e}{e}\left[\frac{1}{2} + \ln\left\{\left(\frac{m_i}{2\pi m_e}\right)^{\frac{1}{2}}(1-\delta)\right\}\right] \tag{17}$$

The secondary electron emission coefficient of boron nitride is given as follows.

$$\delta = 0.1983 \times \left(\frac{kT_e}{e}\right)^{0.576} \tag{18}$$

Figure 3 shows the secondary electron emission coefficient Eq.(18) and the wall potential Eq.(17) as a function of electron temperature. Figure 4 shows the ion flux Eq.(14) and the electron energy flux Eq.(16) to channel wall as a function of electron temperature. When the emission coefficient is above 0.997 (T_e>16.5 eV), the wall potential becomes positive. Then, the wall losses intensively become large.

The following popular frequencies of ionization collision, electron-neutral elastic collision, and Bohm diffusion are used.

Ionization collision frequency:

$$\nu_{ion} = n_n \sigma_0 \sqrt{\frac{8kT_e}{\pi m_e}}\left(1 + 2\frac{kT_e}{E_i}\right)\exp\left(-\frac{E_i}{kT_e}\right) \tag{19}$$

$\sigma_0 = 3.6 \times 10^{-20}\left(m^2\right)$ (Ionization collision cross section)

$E_i = 12.1(eV)$ (Ionization energy of xenon)

$_i$ = 2.5 (Factor of additional energy loss by ionization)

Electron-neutral elastic collision frequency:

$$\nu_{en} = n_n \sigma_{en} \sqrt{\frac{8kT_e}{\pi m_e}} \tag{20}$$

$\sigma_{en} = 2.7 \times 10^{-19}\left(m^2\right)$ (Electron-neutral collision cross section)

Bohm diffusion (anomalous diffusion):

$$\alpha_B \omega_B = \alpha_B \times \frac{eB}{m_e} \qquad (21)$$

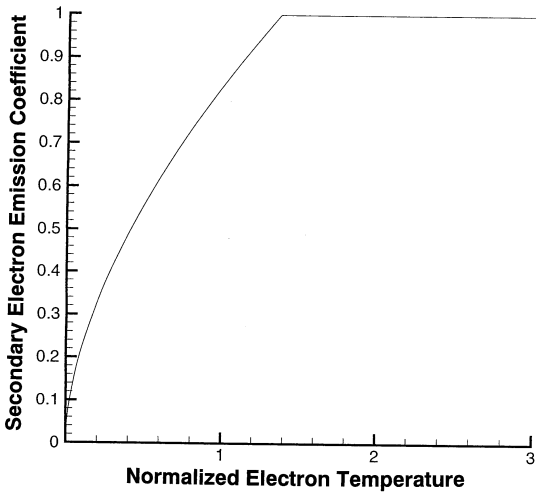

(a) Secondary electron emission coefficient.

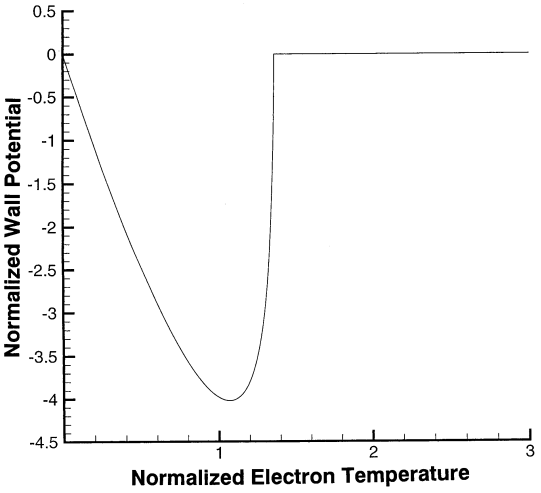

(b) Wall potential.

Fig.3 Secondary electron emission coefficient of boron nitride by electron collision and wall potential on plasma potential depending on electron temperature. The wall potential and electron temperature are normalized with 12.1 V (eV) of xenon ionization voltage (energy). (a) Secondary electron emission coefficient; (b) Wall potential.

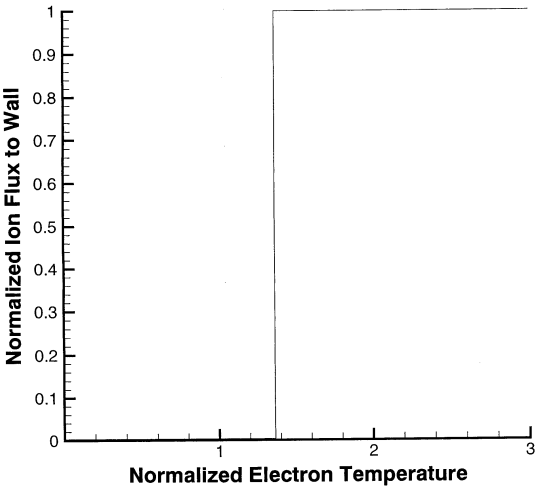

(a) Ion flux.

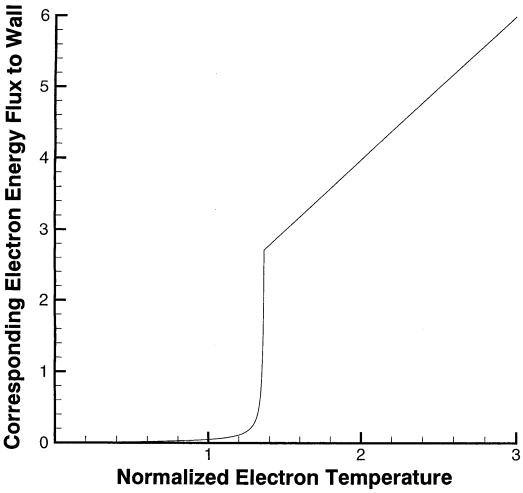

(b) Electron energy flux.

Fig.4 Ion flux and electron energy flux to acceleration channel wall depending on electron temperature. The electron temperature is normalized with 12.1 eV. The ion flux and the electron energy flux are divided by $(kT_e/2\ m_e)^{1/2}n_e$ of thermal velocity flux. (a) Ion flux; (b) Electron energy flux.

After all equations are normalized, numerical integration is carried out under a given operational condition of mass flow rate Eq.(9) and discharge voltage Eq.(7), although the discharge voltage is iteratively obtained with changing discharge current Eq.(5). The ordinary differential equations Eqs.(1) and (2) with some axial distribution of electron temperature are integrated downstream from the upstream end using the four-order Runge-Kutta method. Equation (3) of electron temperature with the fixed axial distributions of electron number density and axial ion velocity is time-dependently calculated using the Euler forward difference scheme with third-order upstream-difference. Hence, a steady-state solution is obtained with the iterative procedure with Eqs.(1)-(3).

An attenuation factor of the present wall losses to the full losses, Eqs.(14) and (16) induced from the negative sheath theory is introduced, and it is $3x10^{-3}$ in this calculation. A Bohm diffusion coefficient is

mainly assumed to be 1/150; that is, a popular value of 1/16 is not used considering experimental data. However, the influences of the coefficient on thruster operational characteristics are also examined with changing it.

3. Results and Discussion

The thruster model for calculation is the THT-IV low power thruster developed in Osaka University[11]. The thruster has an acceleration channel with an outer diameter of 70 mm and an inner diameter of 42 mm, i.e., with 14 mm in width, and the channel length can be changed from 15 to 30 mm. The thruster has magnetic coils on the central axis and on the inner surface of the outer cylinder. Because the two coil currents can be separately controlled, magnetic field shape and strength in the acceleration channel can be changed in order to find out optimum magnetic field structure. Figure 5 shows the axial variation in magnetic field strength with an inner coil current of 1 A and an outer one of 1 A. The magnetic field strength decreases as distance to the anode decreases, and it has a maximum near the channel exit and a minimum at the anode.

In the present calculation, the inner and outer coil currents are changed with a ratio of their coil currents of 1:1 at a discharge voltage of 200 V and a xenon mass flow rate of 2 mg/s. The maximum magnetic field strength near the channel exit is changed from 100 to 200 Gauss although the field shape is not changed. Furthermore, the acceleration channel length is changed from 15 to 35 mm. The cathode is assumed to be located at 10 mm downstream from the channel exit.

3.1 Influences of Magnetic Field Strength

3.1.1 Plasma characteristics dependent on magnetic field strength

Figure 6 shows the axial variations in physical properties dependent on maximum magnetic field strength with an acceleration channel length of 30 mm at a discharge voltage of 200 V and a corresponding mass flow rate of 2 mg/s. The ion flux is normalized with a corresponding flux calculated from the mass flow rate and the channel cross-sectional area. The neutral number density shown in Fig.6(a) rapidly decreases downstream in axial positions from -20 to -12 mm, and the electron number density shown in Fig.6(b) intensively increases downstream in the upstream region of the channel. Ionization is enhanced in the region. As a result, the electron number density characteristics have peaks near -12 mm regardless of magnetic field strength. At axial positions downstream from -18 mm the neutral density increases with magnetic field strength although it slightly decreases in the upstream region. On the other hand, at most of positions inside the channel the electron density decreases with increasing magnetic field strength although it slightly increases near the anode and outside the channel. The electron temperature distributions, as shown in Fig.6(c), also have peaks near the channel exit as well as the electron density characteristics. The electron temperature decreases with an increase in magnetic field strength at axial positions downstream from -15 mm although it slightly increases in the upstream region. The plasma potential shown in Fig.6(d) rapidly decreases downstream from about -15 mm, and then the ion velocity shown in Fig.6(e) increases.

When the magnetic field strength increases, the plasma potential decreases at a constant axial position; i.e., with a stronger magnetic field a decrease in potential begins at a more upstream position. An increase in magnetic field strength raises ion velocity at axial positions from -30 to +5 mm although it decreases ion velocity in the downstream region. In normalized ion flux as shown in Fig.6(f), after it rapidly increases downstream near -15 mm, it gradually increases to about 1.0 in the downstream region. The ion flux decreases with increasing magnetic field strength at axial positions downstream from -15 mm although it slightly increases in the upstream region.

Generally, ions are produced in an upstream region from the anode to about -15 mm, and then they are intensively accelerated in a region downstream just from the ionization region. When the magnetic field strength increases in the channel, ionization occurs in a more upstream region, and ion acceleration begins in the same region; that is, ionization and acceleration overlap in the relatively long region. On the other hand, with a weak

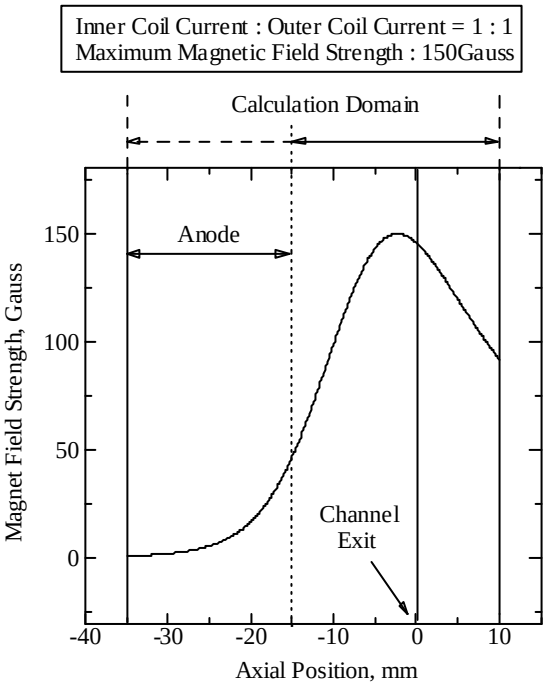

Fig.5 Axial variation in magnetic field strength in acceleration channel of THT-IV Hall thruster.

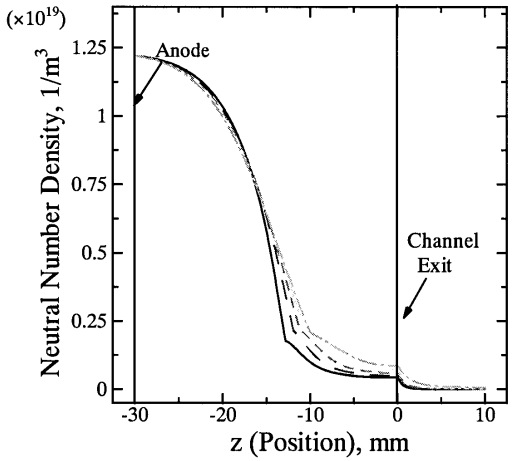

(a) Neutral number density.

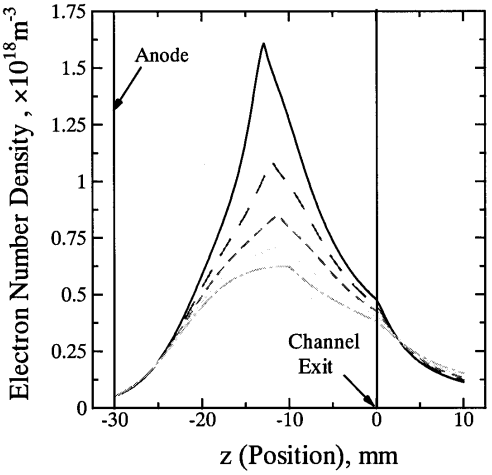

(b) Electron number density.

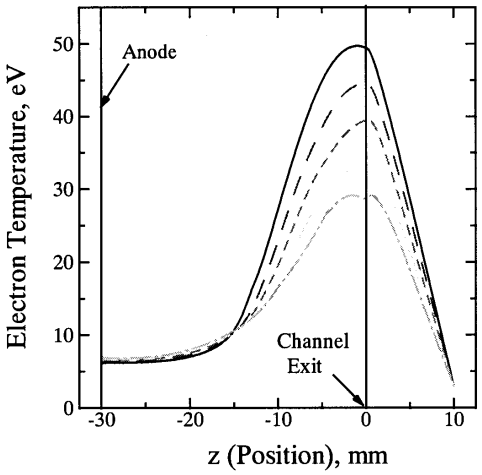

(c) Electron temperature.

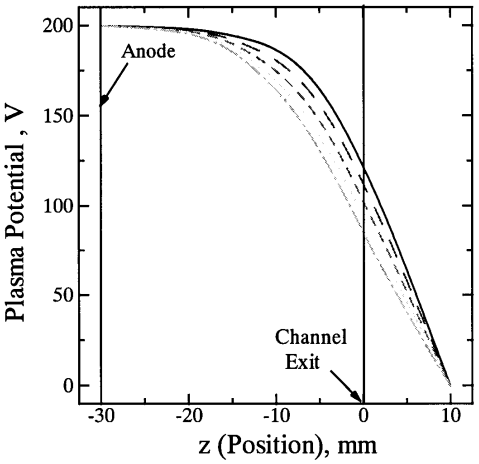

(d) Plasma potential.

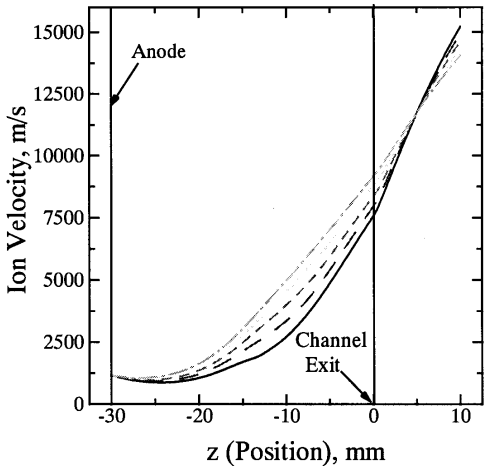

(e) Ion velocity.

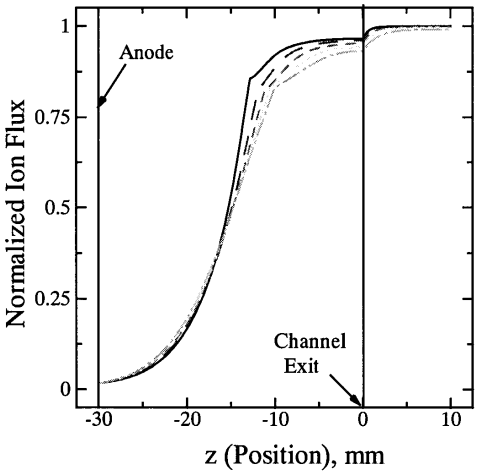

(f) Ion flux.

Maximum Magnetic Field Strength
100Gauss
125Gauss
150Gauss
175Gauss
200Gauss

Fig.6 Calculated axial variations in physical properties dependent on maximum magnetic field strength with

acceleration channel length of 30 mm at discharge voltage of 200 V and corresponding mass flow rate of 2 mg/s. The ion flux is normalized with a corresponding flux calculated from the mass flow rate and the channel cross-sectional area.

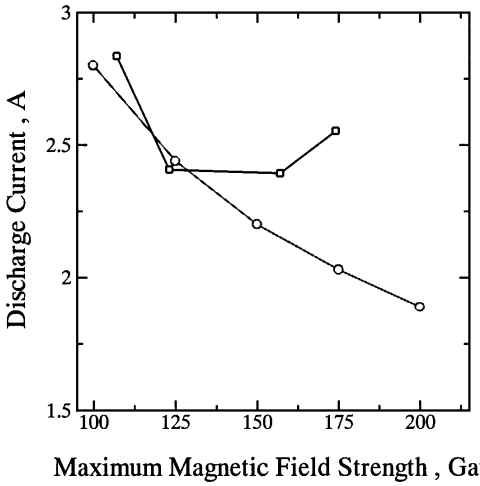

(a) Discharge current.

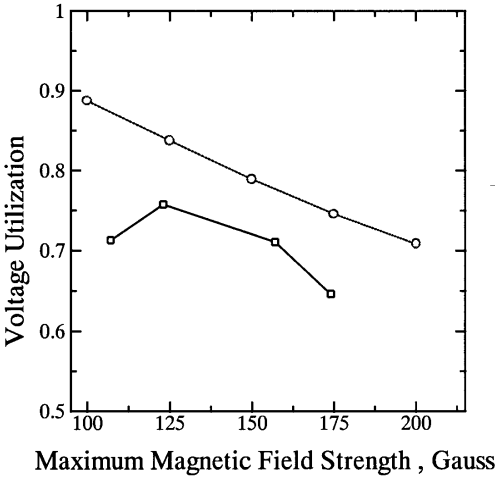

(a) Voltage utilization efficiency.

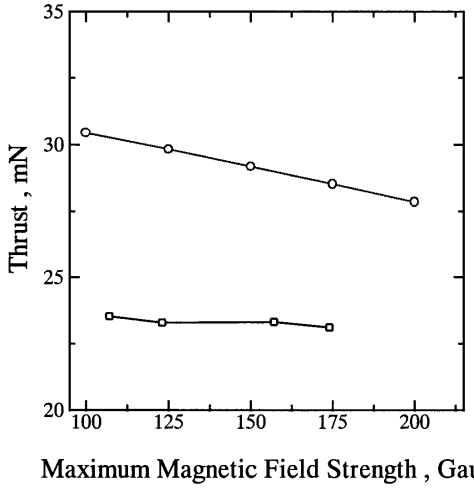

(b) Thrust.

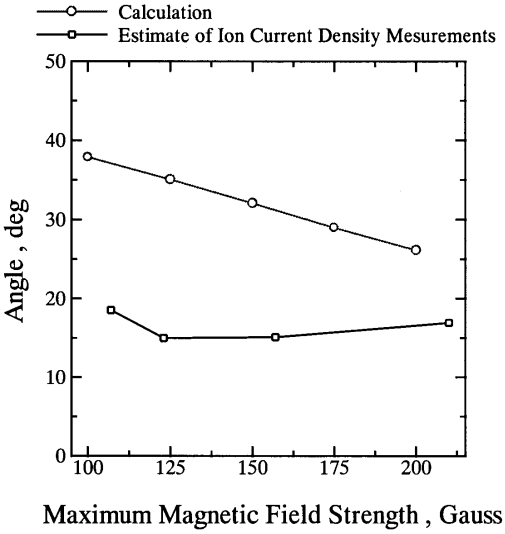

(b) Plasma plume divergent half-angle.

Fig.8 Voltage utilization efficiency and plasma plume characteristics dependent on field strength with 30 mm at 200

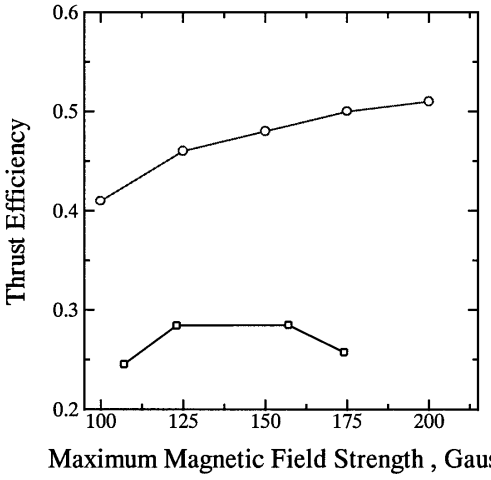

(c) Thrust efficiency.

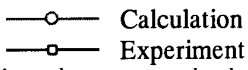

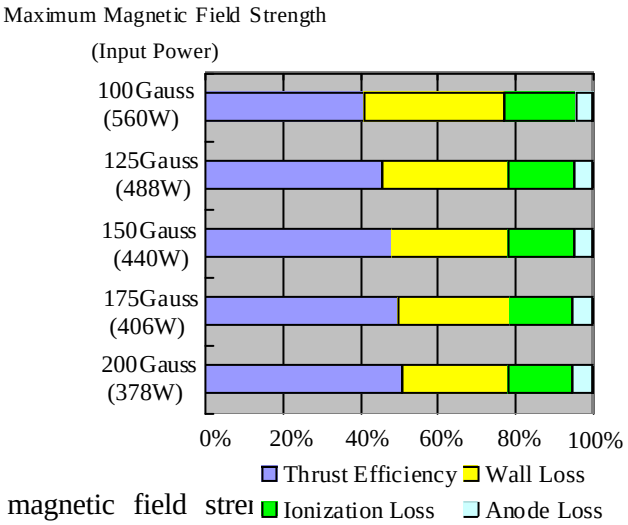

Fig.7 Comparison between calculated and measured magnetic field strei length of 30 mm at discharge voltage of 200 V and thruster performances dependent on maximum

corresponding mass flow rate of 2 mg/s.

Fig.9 Calculated energy balances dependent on maximum magnetic field strength with acceleration channel length of 30 mm at discharge voltage of 200 V and corresponding mass flow rate of 2 mg/s.

magnetic field ion production and acceleration, intensively and efficiently, occur in their thin regions.

3.1.2 Comparison with measured operational characteristics

Figure 7 shows the comparison between calculated and measured thruster performances dependent on maximum magnetic field strength with an acceleration channel length of 30 mm at a discharge voltage of 200 V and a corresponding mass flow rate of 2 mg/s. As shown in Fig.7(a), the calculated discharge current decreases with increasing magnetic field strength. This is because an axial mobility of electrons shown in Eq.(4) becomes smaller with a stronger magnetic field. On the other hand, although the measured discharge current decreases with an increase in magnetic field strength to about 150 Gauss, it increases with above 150 Gauss. The calculated current almost equals the measured one with weak magnetic fields of 100 and 125 Gauss. In cases with the strong magnetic fields, an anomalous diffusion of electrons is expected to occur, as inferred from several experimental data. Although it remains unclear, we can fit a calculated discharge current to the measured one by changing a Bohm diffusion coefficient as shown below.

The calculated thrust, as shown in Fig.7(b), gradually decreases with increasing magnetic field strength. This is because the axial ion velocity, as shown in Fig.6(e), becomes lower outside the channel with a stronger magnetic field. On the other hand, the measured thrust also decreases although the ratio of decrease is small. However, the calculated thrust is much higher than the measured one, and the difference is about 5 mN with all magnetic field strengths.

As shown in Fig.7(c), the calculated thrust efficiency gradually increases with magnetic field strength. This is because the discharge current rapidly decreases and then the input power decreases although the thrust slowly decreases. On the other hand, the measured thrust efficiency has a peak near 150 Gauss, the characteristic qualitatively agrees with the calculated one with the weak magnetic fields. The calculated thrust efficiency is much higher than the measured one at a constant magnetic field strength, and the difference is about 15 % with all magnetic field strengths. This is expected because production of double-charged ions is not considered in this calculation model. Otherwise, we may need to improve the present wall loss model.

Figure 8 shows the voltage utilization efficiency and plasma plume divergent half-angle characteristics dependent on maximum magnetic field strength. The calculated voltage utilization efficiency, as shown in Fig.8(a), decreases with increasing magnetic field strength. The characteristic roughly agrees with the measured one. The decrease in thrust shown in Fig.7(b) is due to the decrease in voltage utilization efficiency. This is because the discharge region in the acceleration channel moves more upstream with a stronger magnetic field. In divergent half-angle shown in Fig.8(b), the calculated one decreases with an increase in magnetic field strength. Although the measured half-angle also decreases in a range of weak magnetic fields, it slightly increases with strong magnetic fields. The calculated half-angle is much larger than the measured one, and the difference is about 20 deg. This is expected because the calculated electron temperature, as shown in Fig.6(c), becomes higher at the channel exit with a stronger magnetic field. We may need to improve the present calculation model of exhaust plasma plume.

Figure 9 shows the calculated energy balances dependent on maximum magnetic field strength. The anode loss presents energy of electrons dissipated into the anode. The thrust efficiency increases with magnetic field strength; the wall loss decreases, and both the ionization loss and the anode loss hardly change. The input power decreases. This is explained as follows. The energy losses of electrons to the channel wall, as shown in Fig.4(b), is a function of electron temperature, and the electron temperature, as shown in Fig.6(c), becomes lower with a stronger magnetic field.

3.2 Influences of Acceleration Channel Length

3.2.1 Plasma characteristics dependent on channel length

Figure 10 shows the axial variations in physical properties dependent on acceleration channel length with a maximum magnetic field strength of 150 Gauss at a discharge voltage of 200 V and a corresponding mass flow rate of 2 mg/s. The neutral number density shown in Fig.10(a) rapidly decreases downstream from some axial position depending on channel length. The rapid decrease in neutral number moves little more upstream with a longer channel. At a constant axial position, the neutral density decreases with increasing channel length. On the other hand, the electron number density shown in Fig.10(b) rapidly increases downstream from the anode; the characteristic has a peak at some axial position, and then the electron density decreases downstream. The peak electron density becomes higher with a longer channel. As a

result, the increase in electron density occurs in a longer distance from the anode as the channel length increases; that is, ionization is enhanced with a long channel. Outside the channel, an increase in channel length decreases the electron density at a constant axial position because it increases the ion velocity as shown in Fig.10(e). In electron temperature shown in Fig.10(c), the characteristic has a peak near the

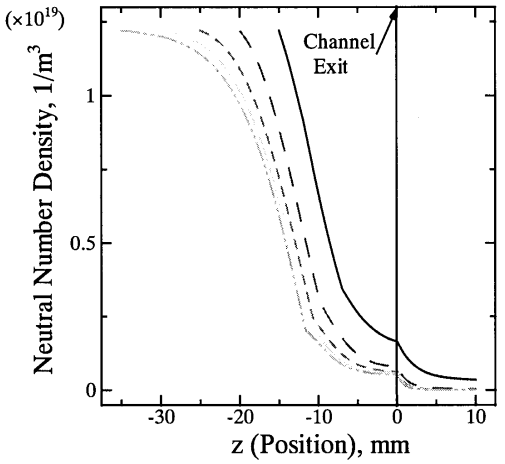

(a) Neutral number density.

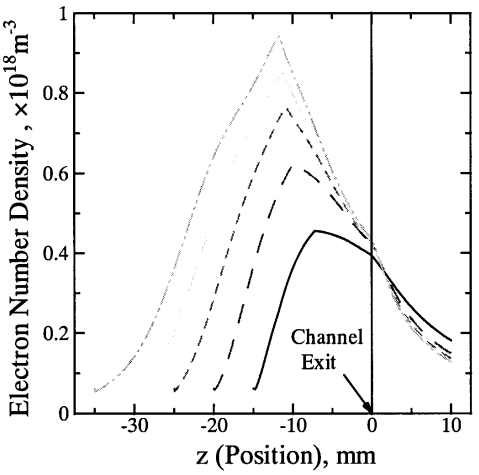

(b) Electron number density.

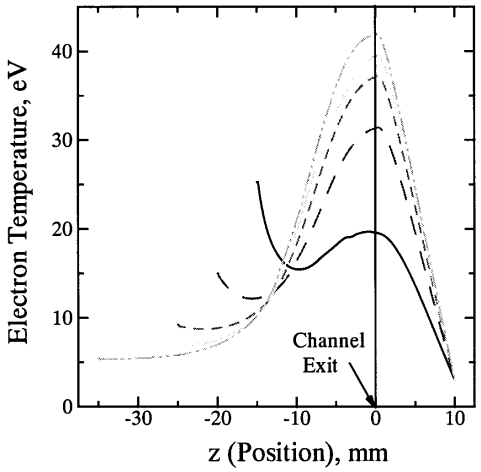

(c) Electron temperature.

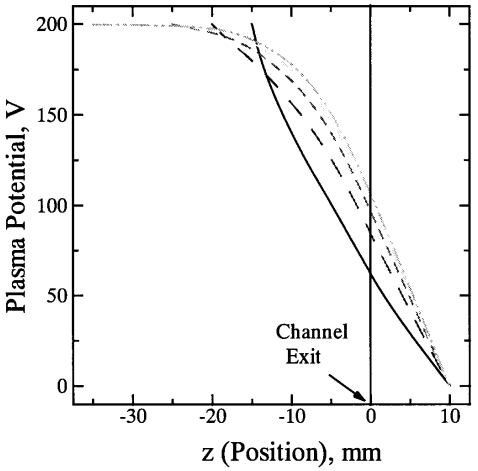

(d) Plasma potential.

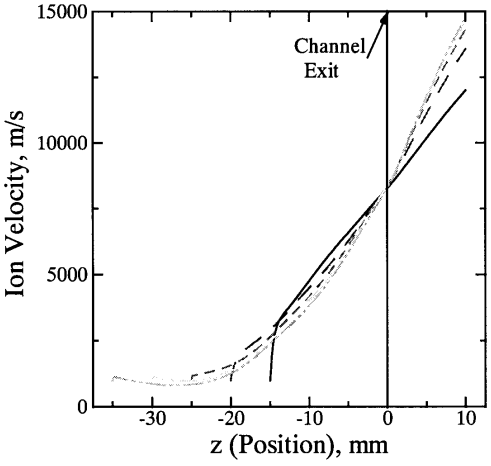

(e) Ion velocity.

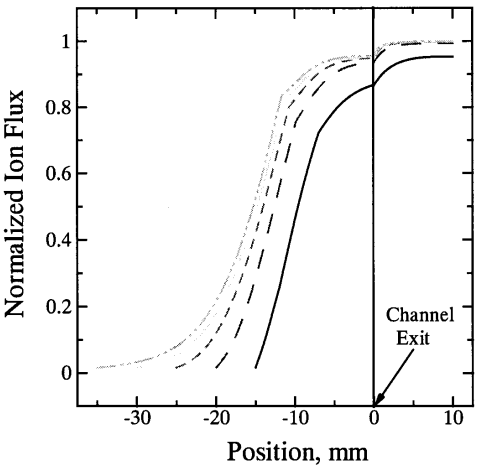

(f) Ion flux.

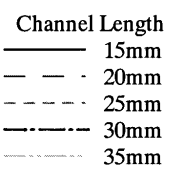

Fig.10 Calculated axial variations in physical properties dependent on acceleration channel length with maximum magnetic field strength of 150 Gauss at discharge voltage of 200 V and corresponding mass flow rate of 2 mg/s. The ion flux is normalized with a corresponding flux calculated from the mass flow rate and the channel cross-sectional area.

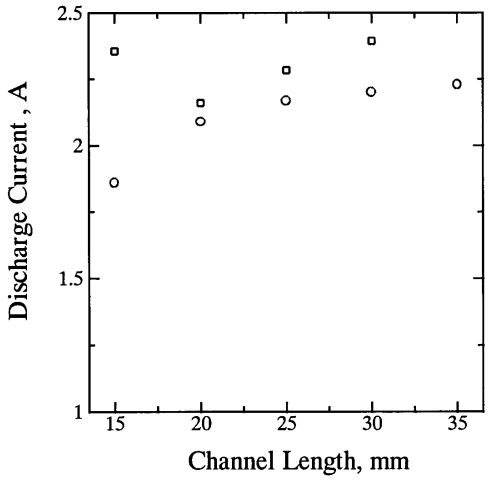

(a) Discharge current.

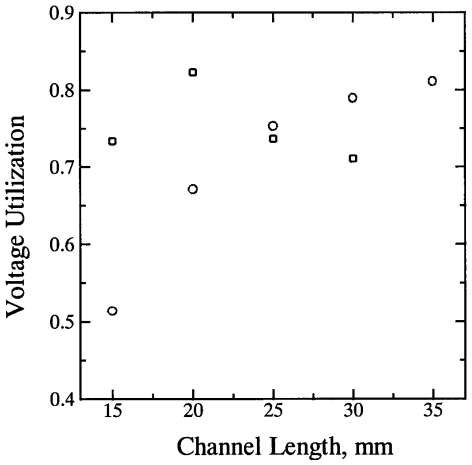

(a) Voltage utilization efficiency.

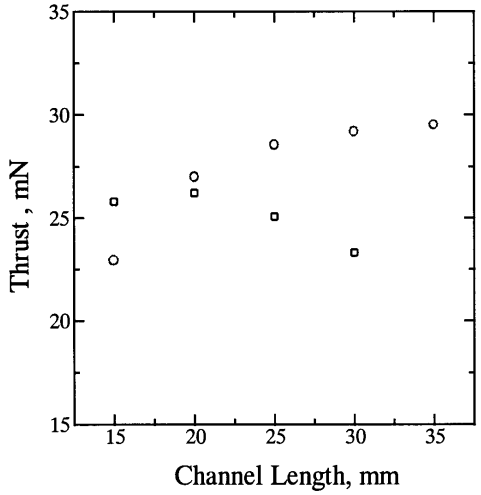

(b) Thrust.

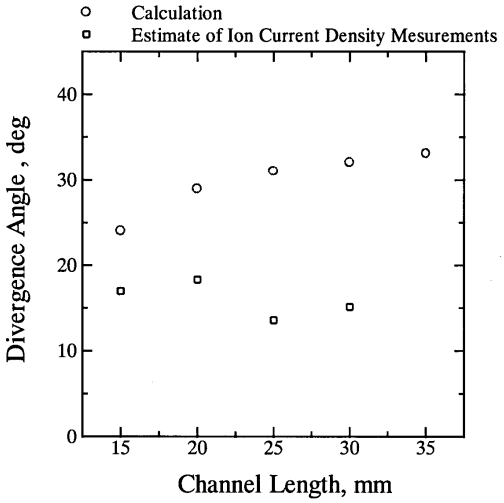

(b) Plasma plume divergent half-angle.

Fig.12 Voltage utilization efficiency and plasma half-angle characteristics dependent hannel length with maximum ength of 150 Gauss at 200 V and

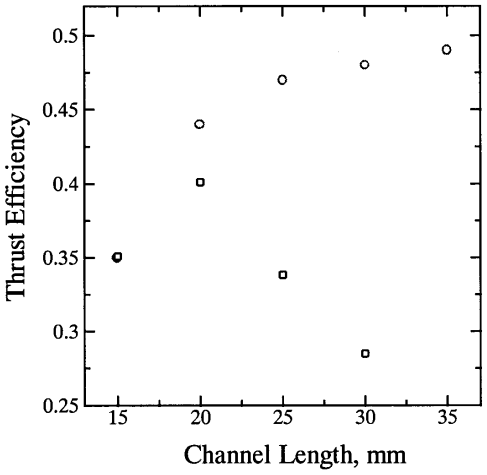

(c) Thrust efficiency.

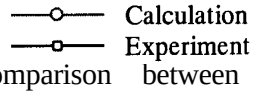

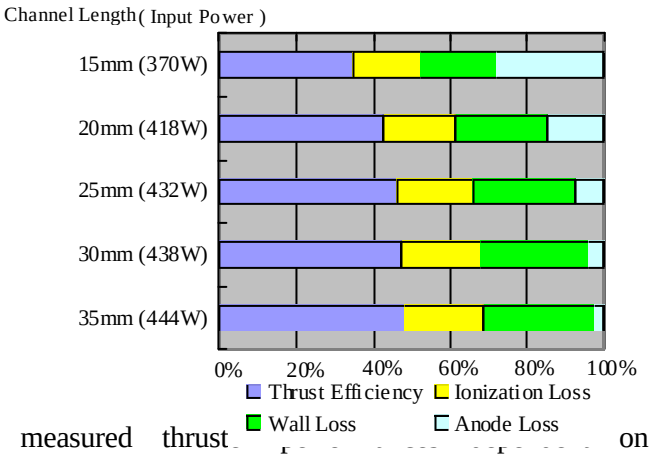

Fig.11 Comparison between calculated and measured thrust on

acceleration channel length with maximum magnetic field strength of 150 Gauss at discharge voltage of 200 V and corresponding mass flow rate of 2 mg/s.

Fig.13 Calculated energy balances dependent on acceleration channel length with maximum magnetic field strength of 150 Gauss at discharge voltage of 200 V and corresponding mass flow rate of 2 mg/s.

channel exit, and the peak temperature becomes higher with a longer channel. With a short channel, the electron temperature increases as approaching the anode. The plasma potential shown in Fig.10(d) rapidly decreases downstream from some axial position. The potential rapidly decreases downstream just from the anode with short channels of 15 and 20 mm in length. However, the potential has a flat characteristic in the upstream region near the anode and then has a drop downstream with large channel lengths of 25, 30 and 35 mm. The ion velocity characteristic agrees with the plasma potential one; i.e., the ion velocity extremely increases in a region corresponding to the rapid decrease in plasma potential. Accordingly, with a long channel the input energy is intensively converted to kinetic energy in the region after rapid ionization. However, with a short channel, some mount of input energy is converted to thermal energy of electrons near the anode, resulting in a high electron temperature near the anode. Outside the channel, the ion velocity increases with channel length at a constant axial position. The ion flux shown in Fig.10(f) also increases downstream as well as the ion velocity. At a constant axial position, the ion flux is higher with a longer channel, and with the shortest channel of 15 mm in length the ion flux does not reach unity at the downstream end; i.e., a fully-ionized condition is not achieved.

Accordingly, with too short channel, ionization begins downstream just from the anode, and then ion acceleration also occurs in the same region. This is because the magnetic field strength is relatively high near the anode, resulting in ion acceleration enhanced near the anode. Furthermore, a number of ions produced is relatively low; i.e., the channel is too short to ionize all neutral particles, although input electric energy is converted to excessive heating of electrons near the anode. In cases of large channel lengths, with a weak magnetic field near the anode, the channel is long enough to produce a fully-ionized plasma, and ion production and acceleration, intensively and efficiently, occur in their regions.

3.2.2 Comparison with measured operational characteristics

Figure 11 shows the comparison between calculated and measured thruster performances dependent on acceleration channel length with a maximum magnetic field strength of 150 Gauss at a discharge voltage of 200 V and a corresponding mass flow rate of 2 mg/s. As shown in Fig.11(a), the calculated discharge current increases with channel length. The calculated current roughly agrees with the measured one except for a case with a channel length of 15 mm. The calculated thrust, as shown in Fig.11(b), also increases with channel length although the measured thrust increases with channel lengths from 15 to 20 mm and slightly decreases in cases with long channels. As a result, the calculated thrust efficiency, as shown in Fig.11(c), gradually increases with channel length although the measured efficiency characteristic has a maximum with 20 mm. The calculated efficiency almost equals the measured one with 15 and 20 mm.

Figure 12 shows the voltage utilization efficiency and plasma plume divergent half-angle characteristics dependent on acceleration channel length. The calculated voltage utilization efficiency, as shown in Fig.12(a), increases with channel length. Because the measured voltage utilization efficiency characteristic has a maximum with 20 mm, it agrees the calculated one with short channels. The increase in thrust with 15 and 20 mm, as shown in Fig.11(b), is due to the increase in voltage utilization efficiency. This is because efficient ion production and acceleration are made with a long channel as mentioned above. In divergent half-angle shown in Fig.12(b), the calculated one increases with an increase in acceleration channel length. The measured half-angle is relatively low with long channels of 25 and 30 mm compared with cases with 15 and 20 mm. The calculated half-angle is much higher than the measured one.

Figure13 shows the calculated energy balances dependent on acceleration channel length. When the thrust efficiency increases with acceleration channel length, the wall loss increases and the anode loss decreases, although the ionization loss hardly change. The input power increases. This is explained as follows. Because a total area of the channel wall increases with channel length, the wall loss ratio increases. On the other hand, the anode loss increases with decreasing channel length because the electron temperature near the anode, as shown in Fig.10(c), increases. As a result, because the decrease in anode loss is superior to the increase in wall loss as increasing channel length, the thrust efficiency increases.

3.3 Dependence of Bohm Diffusion Coefficient

Figure 14 shows the comparison between calculated and measured operational characteristics as varying Bohm diffusion coefficient with an acceleration channel length of 30 mm at a discharge voltage of 200 V and a corresponding mass flow rate of 2 mg/s. In Figs.7(a), the discharge current calculated with a constant Bohm diffusion coefficient of 1/150 is very different from the measured one with strong magnetic fields

above 150 Gauss, resulting from unclear phenomena of electron diffusions. We try to include the unclear anomalous electron diffusions by changing a Bohm diffusion coefficient at each high magnetic field strength. In Fig.14, the characteristics at 100 and 125 Gauss are calculated with a Bohm diffusion coefficient of 1/150, at 150 Gauss with 1/120 and at 175 Gauss with 1/95. The calculated discharge current

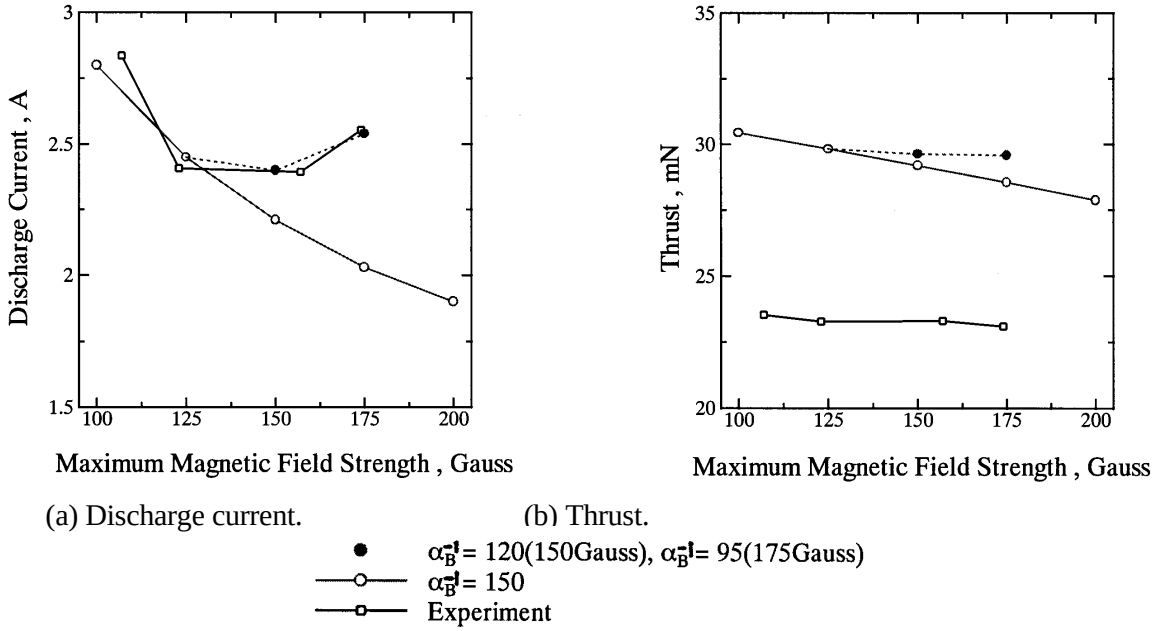

Fig.14 Comparison between calculated and measured operational characteristics as varying Bohm diffusion coefficient with acceleration channel length of 30 mm at discharge voltage of 200 V and corresponding mass flow rate of 2 mg/s.

almost equals the measured one; i.e., its characteristic has a minimum at 150 Gauss. The thrust characteristic also agrees well with the measured one although the large difference still exists. Accordingly, although physical explanation can not be made, the measured performance characteristics with the unclear phenomena may be able to be simulated numerically with the present simple calculation model.

4. Conclusions

Low-power Hall thruster flowfields were calculated using a simple one-dimensional model to understand plasma characteristics and ion acceleration processes and to predict thruster performance. The influences of magnetic field strength and acceleration channel length were mainly examined. The thruster model for calculation is the THT-IV low power thruster developed in Osaka University. Generally, ions were produced in an upstream region from the anode to some axial location of the acceleration channel, and then they were intensively accelerated in a region downstream just from the ionization region. When the magnetic field strength increased in the channel, ionization occurred in a more upstream region, and ion acceleration began in the same region; that is, ionization and acceleration overlapped in the relatively long region. On the other hand, with a weak magnetic field ion production and acceleration, intensively and efficiently, occurred in their thin regions. With too short channel, ionization began downstream just from the anode, and then ion acceleration also occurred in the same region. This is because the magnetic field strength was relatively high near the anode, resulting in ion acceleration enhanced near the anode. Furthermore, a number of ions produced was relatively low; i.e., the channel was too short to ionize all neutral particles. In cases of large channel lengths, with a weak magnetic field near the anode, the channel was long enough to produce a fully-ionized plasma, and efficient ion production and acceleration occurred. The calculated thruster performance agreed with the calculated voltage utilization efficiency, plasma plume divergent half-angle and energy balance characteristics as well as the distributions of physical properties in the channel. However, because the measured performance characteristics did not agree well with the calculated ones, we need to improve the present calculation model, specially modeling of channel wall losses and exhaust plasma plumes. Furthermore, we tried to include the unclear anomalous electron diffusions by changing a Bohm diffusion coefficient at each high magnetic field strength in order to fit a calculated performance to the measured one. The calculated discharge current almost equaled the measured one; i.e., its characteristic has a minimum.

The thrust characteristic also agreed well with the measured one. Accordingly, the measured thruster performance with the unclear phenomena may be able to be simulated numerically with the present simple model.

References

[1] Kim, V.," Main Physical Features and Processes Determining the Performance of Stationary Plasma Thrusters," Journal of Propulsion and Power, Vol.14, pp.736-743, 1998.

[2] Dunning, J.W., Benson, S. and Oleson, S.," NASA's Electric Propulsion Program," 27th International Electric Propulsion Conference, Pasadena, Paper No.IEPC 01-002, 2001.

[3] Cadiou, A, Gelas, C., Darnon, F., Jolivet, L. and Pillet, N.," An Overview of the CNES Electric Propulsion Program," 27th International Electric Propulsion Conference, Pasadena, Paper No.IEPC 01-008, 2001.

[4] Tahara, H., Nikai, Y., Yasui, T. and Yoshikawa, T.," Hall Thruster Research at Osaka University," 35th AIAA/ASME/SAE/ASEE Joint Propulsion Conference and Exhibit, Los Angeles, AIAA Paper No.99-2570, 1999.

[5] Goto, D., Tahara, H., Nikai, Y., Yasui, T. and Yoshikawa, T.," Research and Development of Hall Effect Thrusters at Osaka University," Proceedings of the 26th International Electric Propulsion Conference, Kitakyushu, Vol.1, Paper No.IEPC 99-121, pp.675-682, 1999.

[6] Tahara, H., Mitsuo, K., Goto, D., Yasui, T. and Yoshikawa, T.," Operating Characteristics of Low Power Hall Thrusters," 22nd International Symposium on Space Technology and Science, Morioka, Paper No.ISTS 2000-b-36p, 2000.

[7] Tahara, H., Goto, D., Yasui, T. and Yoshikawa, T.," Thrust Performance and Plasma Characteristics of Low Power Hall Thrusters," 27th International Electric Propulsion Conference, Pasadena, Paper No.IEPC 01-042, 2001.

[8] Shirasaki, A., Tahara, H. and Martinez-Sanchez, M.," One-Dimensional Flowfield Calculation of Hall Thrusters," 23rd International Symposium on Space Technology and Science, Matsue, Paper No.ISTS 2002-b-33p, 2002.

[9] Kitano, T., Fujioka, T., Shirasaki, A., Goto, D., Tahara, H., Yasui, T., Yoshikawa, T., Fuchigami, K., Iinoya, F. and Ueno, F.," Research and Development of Low Power Hall Thrusters," 23rd International Symposium on Space Technology and Science, Matsue, Paper No.ISTS 2002-b-18, 2002.

[10] Kuninaka, H.," Activities on Electric Propulsion in Japan -Space Flight from Basic Research-," 38th AIAA/ASME/SAE/ASEE Joint Propulsion Conference and Exhibit, Indianapolis, AIAA Paper No.2002-3563, 2002.

[11] Tahara, H., Fujioka, T., Kitano, T., Shirasaki, A. and Yoshikawa, T., Fuchigami, K., Iinoya, F. and Ueno, F.," Optimization on Magnetic Field and Acceleration Channel for Low Power Hall Thrusters," 28th International Electric Propulsion Conference, Toulouse, Paper No.IEPC 03-015, 2003.

[12] Ahedo, E., Martinez, P., Gallardo, J.M. and Martinez-Sanchez, M.," Characterization of the Plasma in a Hall Thruster," 27th International Electric Propulsion Conference, Pasadena, Paper No.IEPC 01-017, 2001.